Supplementary Material for "Slow down of the electronic relaxation close to the Mott transition"

Sharareh Sayyad[1,2] and Martin Eckstein[1,2]

[1] *Max Planck Institute for the Structure and Dynamics of Matter, 22761 Hamburg, Germany*
[2] *University of Hamburg-CFEL, 22761 Hamburg, Germany*

(Dated: August 12, 2016)

ANDERSON IMPURITY MODEL: SLAVE-ROTOR DECOMPOSITION

In this section, we present some technical details of the nonequilibrium DMFT solution of the Hubbard model

$$H = -J(t)\sum_{\langle ij\rangle,\sigma}(c^\dagger_{i\sigma}c_{j\sigma}+h.c.)+U\sum_i(n_{i\uparrow}-\tfrac{1}{2})(n_{i\downarrow}-\tfrac{1}{2}), \tag{1}$$

with the slave-rotor representation of the Anderson impurity model, generalizing Ref. [1] to the Keldysh framework. Here $J(t)$ is the time-dependent hopping amplitude,and U is the Hubbard strength.

Within DMFT, the mapping of the lattice problem Eq. (1) onto the impurity model will lead us to the action [2]

$$\mathcal{S} = -i\int_{\mathcal{C}}\mathrm{dtdt}'c^\dagger(t)\Delta(t,t')c(t')+\mathcal{S}_{\rm loc} \tag{2}$$

where

$$\mathcal{S}_{\rm loc} = -i\int_{\mathcal{C}}\mathrm{dt}U\big(n_\downarrow-\frac{1}{2}\big)\big(n_\uparrow-\frac{1}{2}\big), \tag{3}$$

$\mathcal{C}$ stands for the Keldysh contour, Δ is the hybridization function of electrons $\Delta(t,t') = J(t)G_{\rm loc}(t,t')J(t')$, where $G_{\rm loc}(t,t') = -i\langle T_{\mathcal{C}}c(t)c^\dagger(t')\rangle$.

Using slave-rotor decomposition, we represent an impurity electron by $c^\dagger_\sigma = f^\dagger_\sigma e^{i\theta}$, where θ is a phase defined in $[0,2\pi)$, associated with an angular momentum $L = -i\partial/\partial\theta$ and f_σ, is a fermionic charge-less operator with spin σ, known as spinon. In this representation, the the projection to the physical Hilbert space is imposed by

$$L = \sum_\sigma\Big(f^\dagger_\sigma f_\sigma-\frac{1}{2}\Big),, \tag{4}$$

and the commutator relations

$$[L(t),\theta(t')] = -i\delta_{\mathcal{C}}(t,t'), \tag{5}$$

$$\{f_\sigma(t),f^\dagger_{\sigma'}(t')\} = \delta_{\sigma\sigma'}\delta_{\mathcal{C}}(t,t'), \tag{6}$$

assure the electron statistics. It is clear from Eqs. (4, 5), that θ is a bosonic field which carries the charge information.

Using slave-rotor representation, we express the impurity action of Eq. (2) as

$$\begin{aligned}\mathcal{S} = -i\Big\{&\int_{\mathcal{C}}\mathrm{dtdt}'f_\sigma(t)e^{-i\theta(t)}\Delta(t,t')f^\dagger_\sigma(t')e^{i\theta(t')},\\ &+\int_{\mathcal{C}}\mathrm{dt}UL^2+\int_{\mathcal{C}}\mathrm{dt}L(t)(-\partial_t)\theta(t)\\ &+\int_{\mathcal{C}}\mathrm{dt}\sum_\sigma f^\dagger_\sigma(t)(-i\partial_t)f_\sigma(t)\\ &-\int_{\mathcal{C}}\mathrm{dt}\lambda\Big(L(t)-\sum_\sigma f^\dagger_\sigma(t)f_\sigma(t)-1\Big)\Big\},\end{aligned} \tag{7}$$

where λ is the time-independent Lagrange-multiplier. To achieve a L-free action, we first replace operators by their corresponding fields and then integrate over L fields.

After introducing a quantum rotor as $X = e^{i\theta}$, with the constrains as $|X|^2 = 1$, which is imposed by a time-dependent Lagrange-multiplier $\eta(t)$, we obtain (ignoring constant terms)

$$\begin{aligned}\mathcal{S} = -i\Big\{&\int_{\mathcal{C}}\mathrm{dtdt}'f_\sigma(t)X^*(t)\Delta(t,t')f^*_\sigma(t')X(t'),\\ &+\int_{\mathcal{C}}\mathrm{dt}\big(-i\partial_t+\lambda\big)X(t)\frac{1}{4U}\big(i\partial_t+\lambda\big)X^*(t)\\ &+\int_{\mathcal{C}}\mathrm{dt}\sum_\sigma f^*_\sigma(t)(-i\partial_t-\lambda)f_\sigma(t)\\ &-\eta\int_{\mathcal{C}}\mathrm{dt}X(t)X^*(t)\Big\},\end{aligned} \tag{8}$$

The impurity model can be solved exactly when the spin-degeneracy N and the number of rotor flavors M is increased from $N=2$ and $M=1$ to infinity, keeping the ratio $\mathcal{N} = N/M$ fixed [1], and this limit provides a qualitatively correct description of the metal-insulator transition. (In our presented results, we fix the parameter $\mathcal{N}=3$, for which the DMFT phase-diagram is quantitatively reproduced [1].)

At half-filling, we set λ to zero, and acquire the Dyson equations of spinon and rotor fields, using Eq. (8), for

$$G_X(t,t') = -i\langle T_{\mathcal{C}}X(t)X^*(t')\rangle, \tag{9}$$

$$G_f(t,t') = -i\langle T_{\mathcal{C}}f_\sigma(t)f^*_\sigma(t')\rangle, \tag{10}$$

as

$$\big(i\partial_t - \mu\big)G_f(t,t') - [\Sigma_f * G_f](t,t') = \delta_{\mathcal{C}}(t,t'), \qquad (11)$$

$$\Big(\frac{-1}{4U}\partial_t^2 + \eta\Big)G_X(t,t') - [\Sigma_X * G_X](t,t') = \delta_{\mathcal{C}}(t,t'), \qquad (12)$$

where $\Sigma_X(t,t') = i\mathcal{N}\Delta(t,t')G_f(t',t)$ and $\Sigma_f(t,t') = i\Delta(t,t')G_X(t',t)$, are rotor and spinon self-energies.

After solving Dyson equations and computing the rotor and spinon's Green's functions, the electron's Green's function is obtained by $G_{\rm loc}(t,t') = iG_f(t,t')G_X(t,t')$, closing the equations with the DMFT self-consistency. Equations (11) and (12) are solved using the Volterra integral techniques described in Ref. [2], and $\eta(t)$ is determined by a predictor-corrector procedure.

ANDERSON MODEL WITHOUT LATTICE SELF-CONSISTENCY

In this section we use the nonequilibrium slave rotor impurity solver to study a fast quench in the single-impurity Anderson model, i.e. the impurity problem of the Hubbard model without DMFT self-consistency. The results will confirm that the slow quasiparticle formation in the Hubbard model, which is described in the main manuscript, is indeed a lattice effect and not a property of the DMFT impurity model alone. We choose an Anderson impurity model at $U = 2$, with the hybridization function $\Delta(t,t') = J(t)G_0(t,t')J(t')$, where G_0 is the local Green's function of a bath with semi-elliptic density of states of bandwidth 4 and inverse temperature $\beta = 65$, and the coupling is ramped from $J(t) = 0$ for $t < 0$ to $J(t) = 0.4$ for $t > 0.25$. In equilibrium (time-independent $J = 0.4$), this parameter regime corresponds to a three-peak structure of the spectral function, where the central (Kondo) peak has a width of approximately 0.25.

In Fig. 1, we plot the electron, spinon and, rotor lesser Green's functions in and out of equilibrium. In contrast to the corresponding behavior in the Hubbard model (c.f. Fig. 3(a) of the main text), all Green's functions are time-translational invariant for short times $t \gtrsim 16$. In addition, the equilibrium results (black points) of the electronic Green's function lie on top of our nonequilibrium data, indicating that the system is equilibrated. This confirms that the spectral functions corresponding to the Kondo peak are retrieved without any apparent bottleneck behavior.

These results also provide a test for the slave-rotor impurity solver, as they are consistent with previous investigations of the dynamics in the Anderson model [4], which show that the buildup of the Kondo-peak is limited by energy-time uncertainty, i.e., the formation of the peak is complete after a time scale $t_K \sim 1/T_K$, where T_K is the width of the peak.

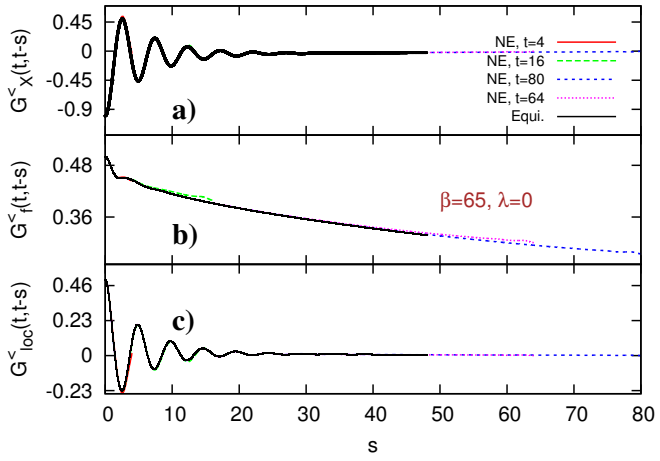

FIG. 1. Lesser components of rotor(a), spinon(b), and electron(c) at three different times $t \in \{16, 64, 80\}$, as well in equilibrium, as a function of time differences. (Anderson impurity model with $U = 2$ and $\beta = 65$, see main text.)

SOLUTION OF THE PROBLEM USING THE NONCROSSING APPROXIMATION

In this section we analyze the quasiparticle formation for the same setup as in the main text, but instead of the slave-rotor decoupling we now use the lowest order strong-coupling expansion [3] (non-crossing approximation, NCA) to solve the DMFT equations. (The implementation of the NCA is described in Ref. [3].) The NCA is known to underestimate the critical interaction U_c of the Mott transition, but nevertheless the method qualitatively reproduces the phase diagram of the Mott transition. It is therefore illustrating to see that also the dynamics of quasiparticle formation described in the main text is captured by the NCA solution.

We use the same setup as in the main text, i.e., the hopping $J(t)$ in the Hubbard model [Eq. (1) of the main text] is suddenly ramped from the atomic limit $J = 0$ to unity $J = 1$, and then the equilibration in a thermal bath of temperature $1/\beta$ is studied. The coupling to the bath is set to $\lambda = 0.5$ throughout this section. Figure 2(a) shows the spectral function in equilibrium ($J = 1$) for various temperatures at $U = 3.1$, which is close to the NCA value for the critical interaction of the metal-insulator transition. The curves show the crossover from the bad metal at high temperatures to the metal with a quasiparticle peak at low temperatures.

Figure 2(b) shows the time-evolution of the spectral function $A(t,\omega) = -\frac{1}{\pi}\mathrm{Im}\int_0^t ds G^{ret}(t-s,t)e^{i\omega s}$ after the ramp-on of the hopping at $t = 0$, which reveals a slow recovery of the quasiparticle peak. In Fig. 2(c) we plot the spectral weight at $\omega = 0$, i.e., the height of the quasiparticle peak, for various temperatures $1/\beta$ of the bath. The final equilibrium height of the quasiparticle peak is recovered within the simulation time only if the temperature is

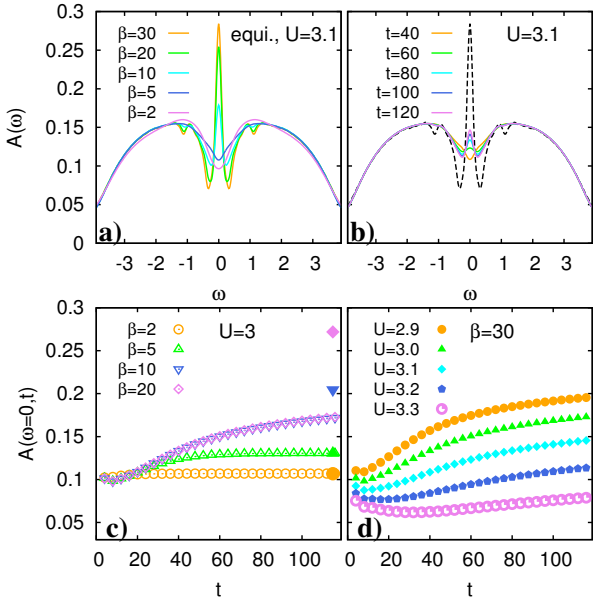

FIG. 2. Similar as Figure 1 of the main text, but using NCA to solve the DMFT equations: (a) Spectral function in equilibrium for various temperatures $U = 3.1$ below the metal insulator transition. (b) Time-dependent spectral function $A(t, \omega)$ after the ramp-on of the hopping, for $U = 3.1$ and inverse bath temperature $\beta = 30$. The dashed line is the equilibrium result. (c) Spectral weight $A(t, \omega = 0)$ at $\omega = 0$ as a function of time for $U = 3$ and inverse bath temperatures β as indicated. The filled symbols correspond the the height $A(\omega = 0)$ of the quasiparticle peak in equilibrium at the same β. (d) Time dependent spectral weight $A(t, \omega = 0)$ at low bath temperature for various interactions U.

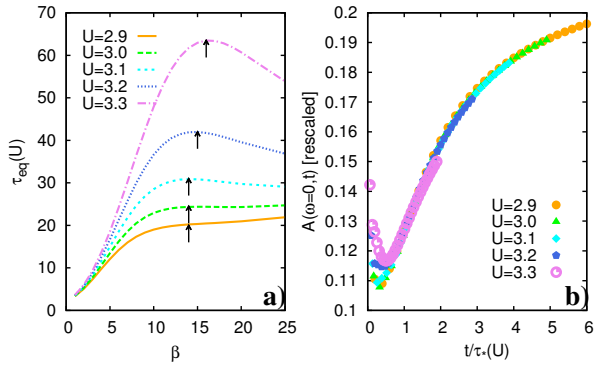

FIG. 3. a) The crossover scale $\tau_{eq}(U, \beta)$ as a function of inverse temperature, obtained using Eq. (13) with the spectral functions obtained within NCA. The arrows point at the maximal or saturated value, used to define the crossover scale $\tau_*(U)$. The resulting values are $\tau_*(U) = 20$ ($U = 2.9$), 24.5 ($U = 3$), 31 ($U = 3.1$), 42 ($U = 3.2$), 63.5 ($U = 3.3$). b) Time dependent spectral weight $A(\omega = 0, t)$ at bath temperature $\beta = 30$ for various interactions U (same data as in Fig 2d) plotted as a function of rescaled time $t/\tau_*(U)$, with the time scale $t/\tau_*(U)$ taken from panel a). Additionally, the curves are rescaled with an arbitrary factor in vertical axis.

above some crossover scale ($\beta = 2, 5$ in Fig. 2(c). At lower temperatures the evolution becomes basically independent of the bath temperature $1/\beta$, whereas the quasiparticle peak in equilibrium would strongly increases with decreasing temperature (the data for $\beta = 10$ and $\beta = 20$ in Fig. 2(c) fall almost on top of each other). Figure 2(d) shows that the evolution becomes slower as U is increased. All this behavior, which indicates the existence of an electronic bottleneck time related to the metal-insulator crossover regime, is therefore perfectly in agreement with the slave-rotor solution (c.f. Fig. 1 of the main text), although shifted to smaller values of the interaction due to the underestimation of the critical U within NCA. (The second order strong-coupling approximation would almost quantitatively yield the phase diagram in equilibrium, but the higher numerical effort does not allow to reach the long simulation times needed to systematically analyze the quasiparticle formation.)

Furthermore, we can investigate whether the slowdown of the dynamics in the NCA solution is determined by the electronic bottleneck time τ_*, which has been identified from the spinon lifetime using the slave-rotor language. Here we extract τ_* from the electronic spectral functions, using the approximate form given by Eq. (4) of the main text. In Fig. 3(a) we show the time scale τ_{eq} obtained by using Eq. (4) of the main text

$$\tau_{\rm eq}^{-1}(\beta) = \int d\omega \, \frac{\pi A(\omega)^2}{\cosh(\beta\omega/2)^2}, \qquad (13)$$

as a function of temperature $1/\beta$, using the DMFT self-consistency for the semi-elliptical density of states, $\Delta(\omega)'' = -\pi A(\omega)$. The maximum or saturation value (black arrows) defines the crossover scale $\tau_*(U)$. In Figure 3(b) we plot the data of Fig. 2(d) as a function of rescaled time $1/\tau_*(U)$, with an additional rescaling of the vertical axis. We observe an approximate data collapse, which confirms that the time-evolution of the quasiparticle height $A(\omega = 0, t)$ for various values of U roughly satisfies a functional form $A(\omega = 0, t) = a_U f(t/\tau_*(U))$ with a given U-independent functional form, analogous to the slave-rotor results represented in Fig. 1(e) of the main text.

COMPARISON TO A PHOTO-EXCITED STATE

In this section we compare the excited state after the J-quench protocol to a photo-excited state. Both after a quench from the atomic limit and after an excitation with a laser pulse (electric field) the system is in a very highly excited state, i.e., the energy per particle corresponds to an effective temperature far above the crossover temperature T^* where we find the slow relaxation dynamics. At these high energies we expect thermalization after a short transient of the order of the bare hopping time (much shorter than the time scales of interest to this work),

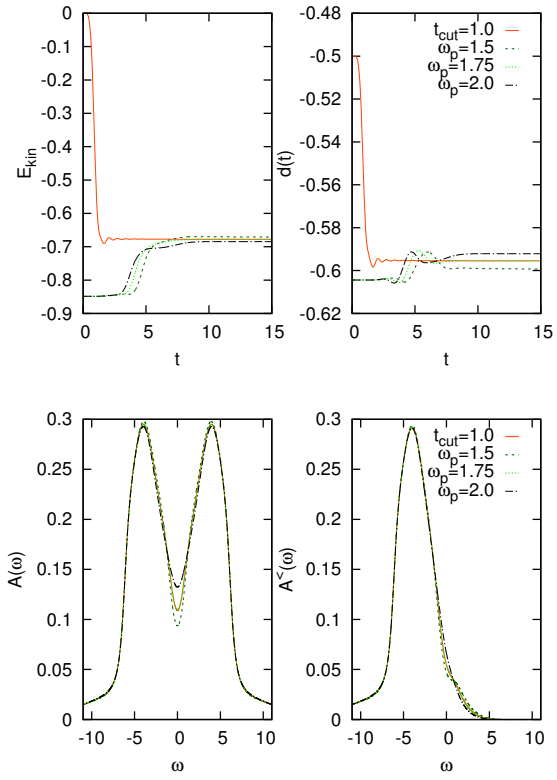

FIG. 4. (a) Kinetic energy and double occupancy after a hopping quench ($t_{\rm cut} = 1$) and excitaton with an electric field pulse (see text) at frequencies $\omega_p = 1.5, 1.75, 2$. (b) Spectral function $A(\omega, t)$ and occupied density of states $A^<(\omega, t)$ at the same parameters, evaluated after a short relaxation time, $t = 15$.

so that both quench and photo-excitation would lead to more or less the same hot-electron state. Rapid thermalization after excitation with an electric field pulse has been observed previously in simulations for the hypercubic lattice [5]. To corroborate the above claim within the Slave-Rotor method, we have simulated both the quench and the laser excitation for the same lattice (a two-dimensional Hubbard model with unit hopping and bandwidth 8). The implementation of the DMFT self-consistency is described in Ref. [5], and we use the slave-rotor impurity solver.

We compare the spectral function $A(t,\omega) = -\frac{1}{\pi}\mathrm{Im}\int_0^t ds\, G^{\rm ret}(t, t-s)e^{i\omega s}$ and the occupied density of states $A^<(t,\omega) = -\frac{1}{2\pi}\mathrm{Im}\int ds\, G^<(t, t-s)e^{i\omega s}$ for two different setups, which are (i), a hopping quench as described in the main text, with a ramp time $t_{\rm cut} = 1$, and (ii), excitation with an electric field along the body diagonal of the lattice, given by a few cycle pulse with frequency ω_p and gaussian envelope, $E(t) = E_0 \sin(\omega_p(t - t_0)) \exp(-4.6(t - t_0)^2/t_0^2)$, where $E_0 = 1$, $t_0 = 2\pi/\omega_p$. Figure 4(a) shows the time-evolution of kinetic energy and double occupancy, and Fig. 4(b) shows the spectral functions. The excitation density is controlled by varying the frequency ω_p. The simulation confirms that if the energy after the excitation is the same ($\omega_p = 1.75$), also the spectral functions after the excitation relax to the same form. As indicated by the form of the spectral function, the final state is in the bad metallic regime far above the onset of the quasi-particle peak. Of course, the scenario of rapid thermalization would break down for weaker excitations, i.e., if the final energy is in the crossover regime where we observed the relaxation bottleneck.

[1] S. Florens and A. Georges, Phys. Rev. B **66**, 165111 (2002).
[2] H. Aoki, N. Tsuji, M. Eckstein, M. Kollar, T. Oka, and Ph. Werner, Rev. Mod. Phys. **86**, 779 (2014).
[3] M. Eckstein and Ph. Werner, Phys. Rev. B **82**, 115115 (2010).
[4] P. Nordlander, M. Pustilnik, Y. Meir, N. S. Wingreen, and D. C. Langreth, Phys. Rev. Lett. **83**, 808 (1999).
[5] M. Eckstein and Ph. Werner, Phys. Rev. B **84**, 035122 (2011).